

# Beyond Entropy: Style Transfer Guided Single Image Continual Test-Time Adaptation

Younggeol Cho\* Youngrae Kim\* Dongman Lee

School of Computing, Korea Advanced Institute of Science and Technology (KAIST)  
Daejeon, Republic of Korea

{rangewing, youngrae.kim, dlee}@kaist.ac.kr

## Abstract

Continual test-time adaptation (cTTA) methods are designed to facilitate the continual adaptation of models to dynamically changing real-world environments where computational resources are limited. Due to this inherent limitation, existing approaches fail to simultaneously achieve accuracy and efficiency. In detail, when using a single image, the instability caused by batch normalization layers and entropy loss significantly destabilizes many existing methods in real-world cTTA scenarios. To overcome these challenges, we present *BESTTA*, a novel single image continual test-time adaptation method guided by style transfer, which enables stable and efficient adaptation to the target environment by transferring the style of the input image to the source style. To implement the proposed method, we devise *BeIN*, a simple yet powerful normalization method, along with the style-guided losses. We demonstrate that *BESTTA* effectively adapts to the continually changing target environment, leveraging only a single image on both semantic segmentation and image classification tasks. Remarkably, despite training only two parameters in a *BeIN* layer consuming the least memory, *BESTTA* outperforms existing state-of-the-art methods in terms of performance. Our code is available at (TBD).

## 1. Introduction

Deep learning models have significantly improved the performance of computer vision applications [6, 14]. However, in real-world scenarios, the models suffer from performance degradation due to domain shifts between training and target data. Unsupervised domain adaptation (UDA) [10, 24, 25, 30, 33, 37, 39] and test-time training (TTT) [23, 38] techniques have been proposed to address the performance gap. These methods assume that the models are adapted to the unseen domain with the huge amount of source data at

\* Equal contribution

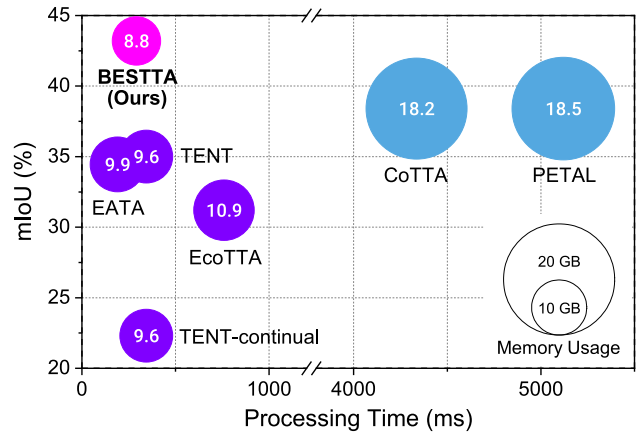


Figure 1. Semantic segmentation performances on the Cityscapes-to-ACDC single image continual test-time adaptation task, evaluated on DeepLabV3Plus-ResNet50 [3]. Processing time includes inference and adaptation time per image. The circle radius and values indicate the peak GPU memory usage. The violet circles are batch normalization-based and the blue circles are pseudo-label-based methods. *BESTTA* significantly outperforms the state-of-the-art continual test-time adaptation methods [1, 28, 36, 41, 43] in terms of mIoU while consuming the least GPU memory.

test time. However it is impractical to utilize these methods in the real world due to the limited computational resources. Fully test-time adaptation (TTA) methods [2, 29, 41] have recently emerged to enable online adaptation of a trained model to the target environment without source data or labels. These TTA methods have limitations in that they can only adapt to a single target domain, resulting in overfitting to the target domain and forgetting the prebuilt knowledge. Consequently, recent studies [1, 28, 36, 43] have proposed continual test-time adaptation (cTTA) methods to adapt a model for continually changing target domains over a long period, addressing the issues of catastrophic forgetting and error accumulation found in the previous TTA methods.

Considering the nature of TTA, a TTA method must ful-

Settings	Data		Learning		Continually Changing Domain	Single Image
	Source	Target	Train stage	Test stage		
Unsupervised Domain Adaptation	$X^s, Y^s$	$X^t$	✓	-	✗	✗
Test-Time Training	$X^s, Y^s$	$X_{\text{batch}}^t$	✓	✓	✗	✗
Fully Test-Time Adaptation	-	$X_{\text{batch}}^t$	-	✓	✗	✗
Continual Test-Time Adaptation	-	$X_{\text{batch}}^t$	-	✓	✓	✗
Single Image Continual Test-Time Adaptation	-	$x_i^t$	-	✓	✓	✓

Table 1. The settings of single image continual test-time adaptation and related adaptation areas.  $X^s$  and  $Y^s$  denote the source image and label sets, respectively,  $X^t$  denotes the target image set,  $X_{\text{batch}}^t = \{x_{i_1}^t, \dots, x_{i+k}^t\}$  denotes the batch of  $k$  target images, and  $x_i^t$  denotes the single target image at time  $i$ .

fill both the efficiency and accuracy requirements of real-world tasks. Meanwhile, real-world downstream vision tasks such as semantic segmentation require the use of high-resolution images for optimal performance [42, 48]. These requirements limit the feasible batch size for edge computing environments where TTA methods are predominantly utilized, owing to the limited computational resources.

Due to the inherent limitations on batch size, existing works have yet to overcome the following two critical limitations, especially when using a *single image* input, as shown in Table 1. Firstly, small mini-batch severely degrades the performances of most existing TTA methods based on batch normalization (BN) [13, 27, 28, 35, 36, 41, 44]. These methods utilize BN to align the distributions between training and target data. However, inaccurate mini-batch statistics cause the substantial performance degradation when using a small batch size, which is more aggravated when dealing with a single image [22, 29]. Secondly, entropy loss, which is employed by the majority of existing TTA methods [13, 19, 31, 36, 41], becomes significantly unstable when only a single image is utilized, due to the large and noisy gradients from the unreliable prediction [29]. In addition, the entropy loss is prone to model collapse by predicting all images into the same class, which minimizes the entropy the most [29]. Although EATA [28] and SAR [29] proposed stabilized versions of entropy loss that filter unreliable samples, these methods still rely on the entropy and do not fully exploit the target samples due to the filtering. Consistency loss using pseudo-labels [1, 43] would overcome this problem, but it is inefficient in terms of computational complexity and memory consumption because it requires multiple inferences for tens of pseudo-labels.

In our paper, we present **BESTTA** (Beyond Entropy: Style Transfer guided single image cTTA), a single image cTTA method that achieves stable adaptation and computational efficiency. First of all, we formulate TTA as a style transfer problem from the target style to the source style. Motivated by the normalization-based style transfer methods [7, 16], we propose BeIN, a single normalization layer that enables stable style transfer of the input. BeIN estimates the proper mini-batch statistics describing the tar-

get domain by incorporating learnable parameters with the source and target input statistics. Moreover, we introduce the style and content losses to ensure effective and stable adaptation while preserving content. Our proposed losses outperform a single entropy loss in terms of stability and efficiency. Second, we implement the style transfer in the simplest form for efficiency. We inject a single adaptive normalization layer, which has only two learnable parameters, into a model, and update a small number of parameters while keeping all model parameters frozen. Finally, we regularize the learnable parameters to prevent overfitting to the continually changing target domain, thereby lead to catastrophic forgetting and error accumulation.

Our contributions are summarized as follows:

- We propose BESTTA, a novel style transfer guided single-image continual test-time adaptation method that enables stable and efficient adaptation. We formulate the test-time adaptation problem as a style transfer and propose novel style and content losses for stable single-image continual test-time adaptation.
- We propose a simple but powerful normalization method, namely BeIN. BeIN provides stable style transfer by learning to estimate the target statistics from input and source statistics.
- We demonstrate that the proposed BESTTA effectively adapts to continually changing target domains with a single image on semantic segmentation and image classification tasks. Remarkably, despite training only two parameters, BESTTA outperforms the existing state-of-the-art methods with the least memory consumption, as shown in Fig. 1.

## 2. Related Work

### 2.1. Test-Time Adaptation

In order to enable model adaptation in source-free, unlabeled, and online settings, various test-time domain adaptation methodologies [2, 19, 22, 29, 29, 31, 41, 46] have been introduced, designing unsupervised losses for this purpose. TENT [41] was the first to highlight the effectiveness of updating batch normalization based on entropy loss in

a test-time adaptation task, inspiring subsequent studies to target batch normalization updates [13, 28, 36]. However, these methods require a large batch size for proper batch normalization statistics and show instability at small batch sizes [22, 29]. While some methods have aimed to facilitate TTA with small batch sizes [19, 22, 29, 31], they often require prior knowledge of domain changes or auxiliary pretraining, making them impractical.

To address this, continual TTA methods [1, 13, 28, 36, 43] have emerged, aiming to prevent catastrophic forgetting and error accumulation caused by continued exposure to the inaccurate learning signal of unsupervised loss. To mitigate these issues, techniques such as stochastic parameter restoration [1, 43] and weight regularization losses [28] have been proposed. However, these methods also lack of considerations for a small batch sizes during adaptation.

## 2.2. Style Transfer

Neural style transfer methods have been proposed to transfer the style of the image while preserving the content [9, 11, 12, 20, 21, 40, 47]. Among them, some studies proposed normalization techniques to effectively transfer the image [7, 16]. Using a similar method, Fahes *et al.* [8] transferred the input styles in a dataset to the target style and trained subsequent neural networks for downstream tasks. Motivated by these methods, we propose to transfer the target feature to the source domain, updating the normalization layer in the cTTA setting.

## 3. Method

Fig. 2 illustrates the overview of the proposed method, BESTTA. Motivated by style transfer methods [7, 16] that use a normalization layer, we formulate the TTA problem as a style transfer problem in Sec 3.1. We propose a single normalization layer, BeIN, which stabilizes the target input statistics in single image cTTA in Sec 3.2, with the proposed losses in Sec 3.3.

### 3.1. Problem Definition

**Stable adaptation on a single image.** Batch normalization (BN) [17] utilizes mini-batch statistics, mean and standard deviation of the source data to normalize data on the same distribution for each channel:

$$\text{BN}(X) = \alpha \cdot \frac{X - \mu_s}{\sigma_s} + \beta \quad (1)$$

where  $X \in \mathbb{R}^{B \times C \times H \times W}$  denotes the mini-batch of input features with  $C$  channels,  $\alpha, \beta \in \mathbb{R}^C$  denote learnable affine parameters optimized during pretraining, and the mean  $\mu_s \in \mathbb{R}^C$  and the standard deviation  $\sigma_s \in \mathbb{R}^C$  are obtained by exponentially averaging the features during pretraining.

TENT [41] introduces the concept of updating affine parameters of BN layers. TENT replaces the source statistics  $(\mu_s, \sigma_s)$  to a target statistics  $(\mu_X, \sigma_X)$  of a target input feature  $X$  to address the distribution shift, and trains the learnable affine parameters  $\alpha$  and  $\beta$  during test-time:

$$\text{BN}_{\text{TENT}}(X) = \alpha \cdot \frac{X - \mu_X}{\sigma_X} + \beta \quad (2)$$

The parameters are updated with the entropy loss  $H(\hat{y}) = -\sum_c p(\hat{y}) \log p(\hat{y})$ , where  $\hat{y}$  is the prediction of the target input. This approach and related studies [28, 36] have demonstrated significant promise in TTA with the large batch size.

However, the normalization-based methods suffer significant performance drop when using small mini-batches, because they depend on the assumption that the true mean  $\mu_t$  and variance  $\sigma_t^2$  of the target distribution can be estimated by the sample statistics. By the central limit theorem, the sample mean  $\mu_X$  follows the Gaussian distribution  $N(\mu_t, \frac{\sigma_t^2}{n})$  for sufficient large samples of size  $n$ . The sample variance follows the Chi-square distribution such that  $(n-1) \frac{\sigma_X^2}{\sigma_t^2} \sim \chi_{n-1}^2$ , and the variance of this distribution  $\text{Var}(\sigma_X^2) = \frac{2\sigma_t^4}{n-1}$ , where the data are normally distributed. Since the variances of the distributions of both sample statistics significantly increase when  $n$  is small, estimating the true mean and variance based on the sample mean and variance becomes difficult, especially for a single image. Therefore, estimating the true mean and variance accurately is required to ensure reliable adaptation with a single image. Also, the entropy loss utilized in these methods is unstable because the instability of BN persists due to its linearity. Furthermore, the entropy loss often results in model collapse, causing biased prediction [29].

Therefore, when dealing with a single image, a solution is required that (1) stabilizes the input statistics in the normalization layers and (2) uses stable losses more than minimizing entropy.

**Test-time adaptation as a style transfer.** In the style transfer domain, there have been several methods that utilize normalization layers for style transfer [7, 16]. Dumoulin *et al.* [7] proposed a conditional instance normalization (CIN) that trains the learnable parameters  $\alpha^s$  and  $\beta^s$  to transfer the style of the encoded input  $x$  to the style  $s$ :

$$\text{CIN}(x; s) = \alpha^s \cdot \frac{x - \mu_x}{\sigma_x} + \beta^s \quad (3)$$

Similarly, AdaIN [16] uses the target style directly in its instance normalization to transfer the style of encoded input  $x$  to the style of encoded target style input  $y$ :

$$\text{AdaIN}(x, y) = \sigma_y \cdot \frac{x - \mu_x}{\sigma_x} + \mu_y \quad (4)$$

where  $\sigma_y$  and  $\mu_y$  denote the standard deviation and mean of the encoded target style input  $y$ . Despite their simplicity,

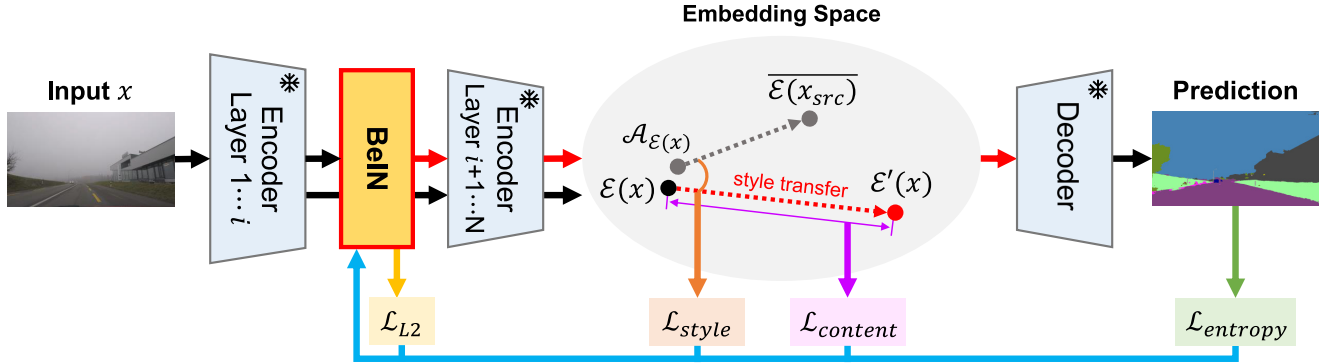


Figure 2. Overview of BESTTA. We inject a single normalization layer, BeIN, to the pretrained model, which facilitates the stable single image continual test-time adaptation via style transfer.  $\mathcal{E}(x)$  denotes the input embedding,  $\mathcal{E}'(x)$  denotes the adapted input embedding,  $\overline{\mathcal{E}(x_{src})}$  denotes the mean source embedding, and  $\mathcal{A}_{\mathcal{E}(x)}$  denotes the exponential moving average of the target embeddings. To transfer the style of the input image to the source style, we adopt the directional style loss  $\mathcal{L}_{style}$ . To avoid the distortion of the content in the input image, we take the content loss  $\mathcal{L}_{content}$ . And to further improve the performance of the model, we use the entropy loss, i.e.,  $\mathcal{L}_{entropy}$ . Finally, to avoid catastrophic forgetting and error accumulation, we use the L2 loss  $\mathcal{L}_{L2}$ . During adaptation, only two normalization parameters in BeIN are trained.

they have shown promising results in style transfer. However, it is important to note that all inputs utilized in the aforementioned methods are in-distribution, which means that the models are trained on both source and target data, therefore the statistics of the encoded input image  $(\mu_x, \sigma_x)$  are reliable. In contrast, cTTA setting involves inputs from an arbitrary target domain that are out-of-distribution, resulting in unreliable and unstable statistics. Motivated by this, we formulate the TTA as a style transfer problem that transfers the target style to the source style:

$$\text{TTA}(x) = \sigma_s \cdot \frac{x - \mu_t}{\sigma_t} + \mu_s \quad (5)$$

where the source and the target domain follow the distributions  $N(\mu_s, \sigma_s^2)$   $N(\mu_t, \sigma_t^2)$ , respectively.

### 3.2. BeIN: BESTTA Instance Normalization

We propose a BESTTA Instance Normalization (BeIN) layer that transfers the style of a target input to the source style, enabling seamless operation of the latter parts of a model. For stability, we estimate the target statistics  $(\mu_t, \sigma_t)$  using an anchor point and learnable parameters  $\gamma_\sigma$  and  $\gamma_\mu$ . We use the source style  $(\overline{\mu_s}, \overline{\sigma_s})$  as the anchor point because it is fixed and therefore stable. The source style contains the mean  $\overline{\mu_s}$  and the standard deviation  $\overline{\sigma_s}$  of the source features, which are small and can be easily obtained from the training phase, before the deployment of our method. BeIN is formulated as:

$$\text{BeIN}(x) = \overline{\sigma_s} \cdot \frac{x - \hat{\mu}_t}{\hat{\sigma}_t} + \overline{\mu_s} \quad (6)$$

where  $\hat{\mu}_t$  and  $\hat{\sigma}_t$  denote the estimated target mean and standard deviation, respectively. We estimate the true target

statistics by combining the target input statistics and the source style. We estimate  $\hat{\sigma}_t$  as a weighted harmonic mean of the source standard deviation and the target input standard deviation with a learnable parameter  $\gamma_\sigma$ :

$$\hat{\sigma}_t = \frac{\overline{\sigma_s} \cdot \sigma_x}{\rho \overline{\sigma_s} + (1 - \rho) \sigma_x + \gamma_\sigma} \quad (7)$$

where  $\rho$  is the hyperparameter that adjusts the ratio of using the source statistics. For the mean, we estimate it by the weighted sum of the source mean and the target input mean with a learnable parameter  $\gamma_\mu$ :

$$\hat{\mu}_t = \rho \frac{\hat{\sigma}_t}{\sigma_x} \cdot \mu_x + (1 - \rho) \frac{\hat{\sigma}_t}{\overline{\sigma_s}} \cdot \overline{\mu_s} + \gamma_\mu \quad (8)$$

The means are scaled with the standard variations to be aligned. We insert BeIN between the layers of the encoder as depicted in Fig. 2. By training only a two parameters in the embedded layer, the latter part of the model seamlessly operates with the preserved prebuilt knowledge, leading to efficient learning and modularization of the whole model.

### 3.3. Style-guided losses

Conventional style losses [7, 11, 16, 21] can be used to guide the learnable parameters in BeIN to transfer the style of the input features to the source style. These style losses align the distribution of the transferred image to the target style. However, they require heavy computations such as additional encoding or decoding processes or computing the gram matrix. Therefore, considering the efficiency requirement of TTA methods, adopting the conventional style losses is impractical. To address this problem, we propose novel directional style loss and content loss that are com-



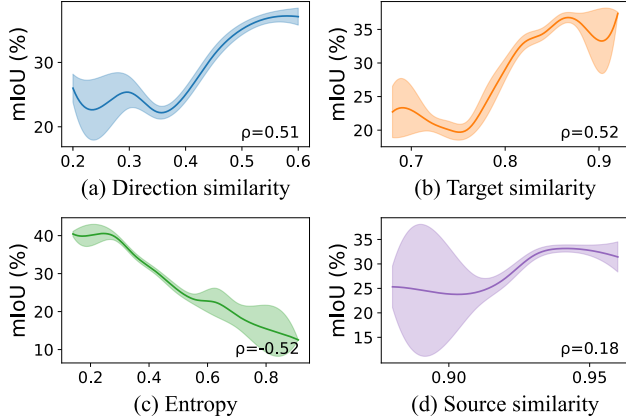


Figure 3. Correlations between performance and style transfer related metrics. We find that direction similarity and target similarity have high correlation ( $\rho > 0.5$ ) with the performance, whereas source similarity [8, 32] is uncorrelated ( $\rho = 0.18$ ). We use the method of Schneider *et al.* [35] to measure the similarity between the adapted and unadapted embeddings. All results are evaluated on the ACDC dataset [34] using DeepLabV3Plus-ResNet50 [4] pretrained on the Cityscapes dataset [5].

puted in the embedding space of encoder during the inference, satisfying efficiency without heavy operations.

**Directional style loss.** Conventional style transfer methods utilize the similarity between an encoded input and an encoded style input. The straightforward solution to our method is to measure the source similarity  $\cos(\overline{\mathcal{E}(x_{src})}, \mathcal{E}'(x))$  [8, 32], that is, the cosine similarity between the adapted target embedding  $\mathcal{E}'(x)$  and the mean source embedding  $\overline{\mathcal{E}(x_{src})}$ . However, as shown in Fig. 3d, we empirically find that the source similarity is not correlated with the performance, thus not beneficial to improve the adaptation. Therefore, motivated by StyleGAN-NADA [9], we devise the directional style loss. We find that the similarity between the adaptation direction  $(\overline{\mathcal{E}(x_{src})} - \mathcal{A}_{\mathcal{E}(x)})$  and the direction from the target to the source  $(\mathcal{E}'(x) - \mathcal{E}(x))$  (see Fig. 2) has high correlation with the adaptation performance as illustrated in Fig. 3a. Therefore, we formulate our directional style loss as follows:

$$\mathcal{L}_{style} = 1 - \cos(\overline{(\mathcal{E}(x_{src}) - \mathcal{A}_{\mathcal{E}(x)})}, (\mathcal{E}'(x) - \mathcal{E}(x))) \quad (9)$$

where  $\mathcal{E}(x)$  is the unadapted target embedding,  $\mathcal{A}_{\mathcal{E}(x)}$  is the exponential moving average of target embeddings.

**Content loss.** Style transfer without consideration about the content of the transferred feature leads to distortion of the contents [11, 16, 21, 47]. Similar to these findings, we find that the target similarity, that is, the cosine similarity between the transferred feature  $\mathcal{E}'(x)$  and the input feature  $\mathcal{E}(x)$  has high correlation with the performance, as shown

in Fig. 3b. Therefore, we devise the content loss as follows:

$$\mathcal{L}_{content} = 1 - \cos(\mathcal{E}(x), \mathcal{E}'(x)) \quad (10)$$

**L2 regularization.** In the continual TTA setting, where long-term adaptation is necessary, it is crucial to prevent catastrophic forgetting and error accumulation to ensure optimal performance. Therefore, we employ an L2 norm to regularize the learnable parameters to prevent overfitting to the current target domain. We formulate the L2 regularization loss as follows:

$$\mathcal{L}_{L2} = \|\gamma_{\mu}\|_2 + \|\gamma_{\sigma}\|_2 \quad (11)$$

**Entropy loss.** We incorporate the entropy loss introduced by Wang *et al.* [41], as BeIN stabilize the normalization. We verify that entropy has strong correlation with the performance on semantic segmentation task as shown in Fig. 3c. The entropy loss is as follows:

$$\mathcal{L}_{entropy} = -\sum p(\hat{y}) \log p(\hat{y}) \quad (12)$$

where  $p$  denotes probability,  $\hat{y}$  denotes prediction.

**Total loss.** We train the learnable parameters in our proposed BeIN layer with a combination of the proposed losses. The total loss  $\mathcal{L}$  is as follows:

$$\mathcal{L} = \lambda_1 \cdot \mathcal{L}_{style} + \lambda_2 \cdot \mathcal{L}_{content} + \lambda_3 \cdot \mathcal{L}_{entropy} + \lambda_4 \cdot \mathcal{L}_{L2} \quad (13)$$

where  $\lambda_1$ ,  $\lambda_2$ ,  $\lambda_3$ , and  $\lambda_4$  are the weights for each loss.

## 4. Experiments

We conduct two experiments on our proposed method in terms of semantic segmentation and image classification. We use the following methods as baselines:

- Fully TTA: BN Stats Adapt [27] and TENT [41]
- Continual TTA: TENT-continual [41], EATA [28], CoTTA [43], EcoTTA [36], and PETAL [1]

### 4.1. Experiments on Semantic Segmentation

We evaluate our proposed method and other baselines in two different settings on semantic segmentation: Cityscapes-to-ACDC continual TTA and Cityscapes-to-Cityscapes-C gradual TTA. All semantic segmentation results are evaluated in mean intersection over union (mIoU).

**Experimental setup.** Following the setting of CoTTA [43], we conduct experiments in the continually changing target environment. We adopt the Cityscapes dataset [5] as the source dataset and the Adverse Conditions (ACDC) dataset [34] as the target dataset. The ACDC dataset includes four different adverse weather conditions (i.e., fog, night, rain, and snow) captured in the real-world. We conduct all experiments without the domain label except for

Time			$t \longrightarrow$																Mean
Method	Memory (GB)	Time (ms)	Round 1				Round 4				Round 7				Round 10				
			Fog	Night	Rain	Snow	Fog	Night	Rain	Snow	Fog	Night	Rain	Snow	Fog	Night	Rain	Snow	
Source	1.76	135.9	44.3	22.0	41.5	38.9	44.3	22.0	41.5	38.9	44.3	22.0	41.5	38.9	44.3	22.0	41.5	38.9	36.6
BN Stats Adapt [27]	2.01	192.7	36.8	<u>23.5</u>	38.2	36.3	36.8	23.5	38.2	36.3	36.8	23.5	38.2	36.3	36.8	23.5	38.2	36.3	33.7
TENT* [41]	9.58	343.8	38.2	22.9	41.1	37.8	38.2	22.9	41.1	37.8	38.2	22.9	41.1	37.8	38.2	22.9	41.1	37.8	35.0
TENT-continual [41]	9.58	343.8	37.7	<u>23.5</u>	39.9	37.5	31.4	17.3	30.7	26.8	19.8	11.2	18.8	17.3	13.4	8.7	12.4	11.8	22.3
EATA [28]	9.90	190.6	36.8	23.4	38.3	36.5	37.6	<u>23.5</u>	39.0	37.1	38.1	<u>23.6</u>	39.5	37.6	38.5	<u>23.6</u>	39.9	38.0	34.4
CoTTA [43]	18.20	4337	<u>46.3</u>	22.0	<u>44.2</u>	40.4	<u>48.1</u>	21.0	<u>45.3</u>	40.2	<u>48.1</u>	20.4	<u>45.3</u>	39.7	<u>48.0</u>	20.0	<u>45.1</u>	39.5	38.4
EcoTTA [36]	10.90	759.3	33.4	20.8	35.6	32.9	34.2	21.2	36.1	33.2	34.7	21.3	36.3	33.2	34.9	21.4	36.5	33.2	31.2
PETAL [1]	18.51	5120	44.7	22.1	42.9	40.1	47.3	22.4	44.4	<u>40.8</u>	47.1	22.1	44.7	<u>40.6</u>	46.9	22.0	44.6	<u>40.5</u>	<u>38.5</u>
BESTTA (Ours)	8.77	291.8	<b>47.8</b>	<b>24.3</b>	<b>47.2</b>	<b>43.8</b>	<b>54.5</b>	<b>26.1</b>	<b>48.4</b>	<b>45.2</b>	<b>54.5</b>	<b>26.1</b>	<b>48.4</b>	<b>45.3</b>	<b>54.5</b>	<b>26.1</b>	<b>48.4</b>	<b>45.3</b>	<b>43.2</b>

Table 2. Semantic segmentation results (mIoU in %) on Cityscapes-to-ACDC single image continual test-time adaptation task. We compare ours with other state-of-the-art TTA methods in terms of peak GPU memory usage (GB) and time consumption (ms) for each iteration, and mean intersection over union (mIoU). All results are evaluated using the DeepLabV3Plus-ResNet50. \* denotes the requirement about when the domain shift occurs. The **best** and second best results are highlighted.

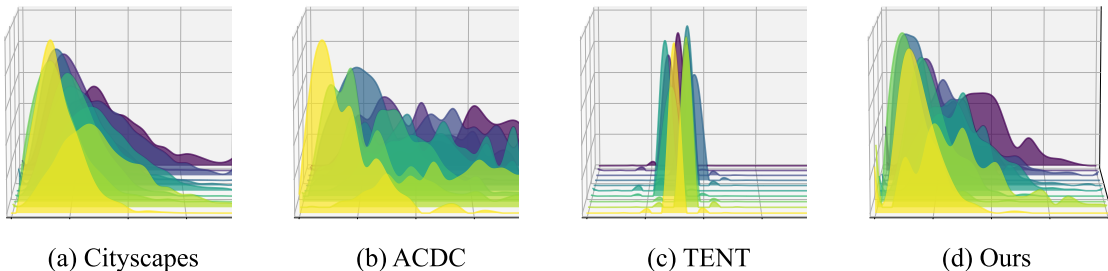


Figure 4. Embedding feature distributions of (a) Cityscapes dataset on Source model, (b) ACDC dataset on Source model, (c) ACDC dataset on TENT, (d) ACDC dataset on our method. Ours aligns the distribution with the source dataset, whereas TENT collapses into a single point. We use DeepLabV3Plus-ResNet50 pretrained on Cityscapes in this experiment.

Time		$t \longrightarrow$				Mean
Method	Bright.	Fog	Frost	Snow		
Source	67.5	59.3	24.8	13.9	41.4	
TENT-continual [41]	61.9	45.2	23.0	15.3	36.3	
PETAL [1]	64.7	35.8	5.7	0.4	26.7	
BESTTA (Ours)	<b>68.2</b>	<b>60.5</b>	<b>31.6</b>	<b>20.0</b>	<b>45.0</b>	

Table 3. Semantic segmentation results (mIoU in %) on the Cityscapes-to-Cityscapes-C gradual test-time adaptation task. All experiments are evaluated using DeepLabV3Plus-ResNet50.

TENT [41]. We repeat the same sequence of four weather conditions 10 times (i.e., fog  $\rightarrow$  night  $\rightarrow$  rain  $\rightarrow$  snow  $\rightarrow$  fog  $\rightarrow \dots$ , 40 conditions in total).

We also conduct experiments in the gradually changing target environment to simulate more realistic environments. We adopt the Cityscapes dataset as the source dataset and the Cityscapes-C dataset [15, 26] as the target dataset. The Cityscapes-C dataset is the corrupted version of the Cityscapes dataset that includes 5 severity levels and 15 types of corruptions. Following EcoTTA [36], we uti-

lize the four most realistic types of corruptions (i.e., brightness, fog, frost, snow) in our experiment. The model faces varying levels of corruption severity for a specific weather type, progressing from 1 to 5 and then from 5 to 1. Once the severity reaches the lowest level, the corruption type is changed (e.g., brightness 1  $\rightarrow$  2  $\rightarrow \dots \rightarrow$  5  $\rightarrow$  4  $\dots \rightarrow$  1  $\rightarrow$  fog 1  $\rightarrow$  2  $\rightarrow \dots$ , 36 conditions in total).

**Implementation Details.** We utilize ResNet50-DeepLabV3+ [3] pretrained on the Cityscapes dataset. We set the batch size to 1 with an image of size  $1920 \times 1080$  for the continually changing setting and a  $2048 \times 1024$  size for the gradually changing setting, respectively. We collect the source style  $(\mu_s, \sigma_s)$  and the mean source embedding  $\mathcal{E}(x_{src})$  by inferencing the source data before deployment. We insert the proposed BeIN layers between the third and fourth layers in the backbone. The  $\lambda_1, \lambda_2, \lambda_3$ , and  $\lambda_4$  are set to 0.3, 1.0, 0.3, and 0.04, respectively. For optimization, we employ the SGD optimizer with a learning rate of 0.001 for the adaptation phase. Note that the model was pretrained with a learning rate of 0.1. The experiments are conducted using an NVIDIA RTX3090 GPU.

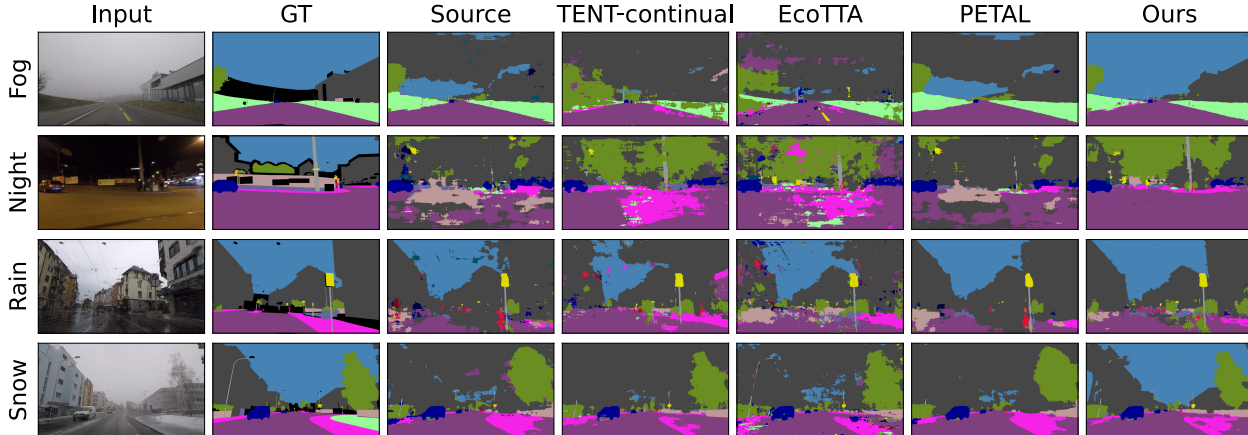


Figure 5. Qualitative comparison of semantic segmentation on Cityscapes-to-ACDC task. All experiments are evaluated using DeepLabV3Plus-ResNet50. The results of other methods are presented in the supplementary material.

$\mathcal{L}_{entropy}$	$\mathcal{L}_{style}$	$\mathcal{L}_{content}$	$\mathcal{L}_{L2}$	Round 1	Round 4	Round 7	Round 10	Mean
✓	✗	✗	✗	21.2	5.3	4.5	4.2	6.7
✓	✓	✗	✗	37.1	32.3	30.2	28.9	31.8
✓	✓	✓	✗	40.1	39.2	37.9	37.3	38.6
✓	✓	✓	✓	<b>40.8</b>	<b>43.5</b>	<b>43.6</b>	<b>43.6</b>	<b>43.2</b>

Table 4. Ablation study on our losses. Performances (mIoU in %) are evaluated on Cityscapes-to-ACDC task for each different combination of losses, using DeepLabV3Plus-ResNet50 [4].

Layer1	Layer2	Layer3	Layer4	mIoU
✓	✗	✗	✗	41.7
✗	✓	✗	✗	40.9
✗	✗	✓	✗	<b>43.2</b>
✗	✗	✗	✓	36.0
✓	✗	✓	✗	43.0
✗	✓	✓	✗	41.7
✗	✗	✓	✓	41.4

Table 5. Ablation study on the position of BeIN. Performance (mIoU in %) are evaluated on Cityscapes-to-ACDC task, using DeepLabV3Plus-ResNet50.

**Quantitative Results.** As shown in Table 2, we compare our approach with the baselines on the cTTA setting. Our proposed BESTTA achieves the highest mIoU across all weather types and rounds. In particular, our method significantly outperforms the second-best baseline, PETAL [1], with a mean mIoU gap of 4.7%, despite using 5.7% of the processing time per image compared to the second-best model. Ours also prevent catastrophic forgetting and error accumulation in the long-term adaptation, as ours shows consistently high performance. In contrast, the BN-based methods [28, 36, 41] show severe performance degradation. Notably, even we reinitialize the TENT reinitialize whenever each domain change occurs, the performance is lower

than the source model. This indicates that the unstable mini-batch statistics and entropy loss hinder the adaptation in single image cTTA.

The experimental results for the gradually changing setting are presented in Table 3. Similar to the cTTA setting, our method significantly outperforms the baselines. All the baselines perform worse than the source model, indicating that they fail to deal with the single image cTTA setting.

**Qualitative Results.** Fig. 4 provides the distributions of the adapted features of ours and the baselines. Comparing Fig. 4a and Fig. 4b, the feature distribution of the target domain that is obtained by the source model is diversified. The distribution of TENT-adapted feature is collapsed into a single point, due to the entropy loss. In contrast, our adapted feature is aligned with the source features from the source model. This indicates that our BESTTA effectively and stably adapts the model to the target domain.

Fig. 5 shows predictions of ours and the baselines on the ACDC dataset. Compared to the other state-of-the-art methods, our results are clearer and more accurate. In particular, at night, the baselines show globally noisy predictions while ours show clear results; in fog and snow, our method perceives the sky as sky while others predict it as buildings. These observations demonstrate the effectiveness of our method in a real-world environment. Further results are presented in the supplementary material.

Time	$t$														Mean	
Method	Gaussian	shot	impulse	defocus	glass	motion	zoom	snow	frost	fog	brightness	contrast	elastic-trains	pixelate		jpeg
Source	88.9	89.2	89.6	77.5	83.2	75.6	77.2	75.2	70.0	68.4	66.9	49.9	81.0	81.2	83.2	77.1
BN Stats Adapt [27]	89.5	89.4	89.7	90.1	89.5	89.5	89.5	89.6	89.6	89.2	89.8	90.1	89.5	89.4	89.6	89.6
TENT-continual [41]	90.0	90.0	90.0	90.0	90.0	90.0	90.0	90.0	90.0	90.0	90.0	90.0	90.0	90.0	90.0	90.0
CoTTA [43]	54.0	64.0	78.0	86.8	88.0	89.9	89.7	87.8	87.6	89.7	88.7	90.0	89.4	53.9	86.7	81.6
PETAL [1]	51.1	52.0	77.7	73.4	62.8	79.7	84.1	48.3	67.4	78.9	19.0	81.5	56.5	57.4	69.8	64.0
BESTTA (Ours)	55.2	50.5	65.6	38.1	46.1	29.3	32.6	23.4	33.1	21.8	9.1	38.5	24.5	44.3	28.9	36.1

Table 6. Image classification results on CIFAR-10-C. All results are evaluated using WideResNet-28 pre-trained on CIFAR-10. We use the error rate (%) as the metric. The **lowest** and second lowest error rates are highlighted.

**Effectiveness of losses.** We perform an ablation study on our losses, and the results are provided in Table 4. Updating the parameters in BeIN only with entropy losses yields the lowest performance. Conversely, including style loss significantly improves performance, demonstrating the effectiveness of style transfer in our method. The addition of content loss further improves performance by preserving the content of the input image, allowing only feature styles to be transferred. However, it still exhibits error accumulation, as evidenced by a gradual performance degradation. L2 loss effectively prevents this phenomenon by maintaining stable performance across rounds.

**Selection of layer to insert BeIN layer.** Table 5 shows the effectiveness of the selection of layers, where the BeIN layer is inserted to transfer the features. Adaptation of features from layer third achieves the highest performance. However, the addition of other layers leads to a performance degradation compared to using only the third layer.

**Prevention of catastrophic forgetting.** As shown in Fig. 6, we evaluated the performance of adapted models after each round on the source dataset, to assess the robustness to the forgetting. TENT exhibits an error accumulation, reflected in the decrease in performance on the ACDC with each round. In addition, TENT experiences catastrophic forgetting of source knowledge, as evidenced by a rapid decline in performance on Cityscapes (the source dataset). In contrast, our method demonstrates resilience against forgetting source-trained knowledge, with remarkably improved performance across all rounds.

## 4.2. Experiments on Image Classification

**Experimental Setup.** We conduct experiments to verify the effectiveness of our method in image classification. Following CoTTA [43], we pretrain the WideResNet-28 [45] on CIFAR-10 [18] and adapt the network to CIFAR-10-C [15] in the single image cTTA setting.

**Results.** As provided in Table 6, our approach outperforms

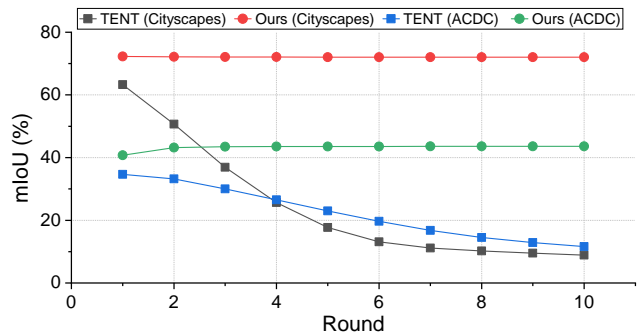


Figure 6. Robustness to catastrophic forgetting. We evaluated the adapted models after each round on the source dataset (Cityscapes). All experiments are evaluated on Cityscapes-to-ACDC in semantic segmentation using DeepLabV3Plus-ResNet50. In comparison to TENT, ours does not show catastrophic forgetting and error accumulation.

other methods in mean accuracy over different corruption types. TENT shows performance that is almost equal to random performance. The second best method, PETAL, is better than the source model, but it is far from satisfactory performance. In contrast, our method exhibits anti-forgetting and maintains high performance over time.

## 5. Conclusion

In this paper, we propose BESTTA, a style transfer guided continual test-time adaptation (cTTA) method for stable and efficient adaptation, especially in the single image cTTA setting. To stabilize the adaptation, we devise a stable normalization layer, coined BeIN, that incorporates learnable parameters and source statistics. We propose style-guided losses to guide our BeIN to effectively transfer the style of the input image to the source style. Our approach achieves state-of-the-art performance and memory efficiency in the single image cTTA setting. We plan to explore a method to automatically select the best layer to insert our BeIN layer.



## References

- [1] Dhanajit Brahma and Piyush Rai. A probabilistic framework for lifelong test-time adaptation. In *Proceedings of the IEEE/CVF Conference on Computer Vision and Pattern Recognition (CVPR)*, pages 3582–3591, 2023. 1, 2, 3, 5, 6, 7, 8
- [2] Dian Chen, Dequan Wang, Trevor Darrell, and Sayna Ebrahimi. Contrastive test-time adaptation. In *Proceedings of the IEEE/CVF Conference on Computer Vision and Pattern Recognition*, pages 295–305, 2022. 1, 2
- [3] Liang-Chieh Chen, Yukun Zhu, George Papandreou, Florian Schroff, and Hartwig Adam. Encoder-decoder with atrous separable convolution for semantic image segmentation. In *Proceedings of the European conference on computer vision (ECCV)*, pages 801–818, 2018. 1, 6, 2, 4, 5, 7
- [4] Liang-Chieh Chen, Yukun Zhu, George Papandreou, Florian Schroff, and Hartwig Adam. Encoder-decoder with atrous separable convolution for semantic image segmentation. In *Proceedings of the European Conference on Computer Vision (ECCV)*, 2018. 5, 7
- [5] Marius Cordts, Mohamed Omran, Sebastian Ramos, Timo Rehfeld, Markus Enzweiler, Rodrigo Benenson, Uwe Franke, Stefan Roth, and Bernt Schiele. The cityscapes dataset for semantic urban scene understanding. In *Proceedings of the IEEE conference on computer vision and pattern recognition*, pages 3213–3223, 2016. 5, 7
- [6] Alexey Dosovitskiy, Lucas Beyer, Alexander Kolesnikov, Dirk Weissenborn, Xiaohua Zhai, Thomas Unterthiner, Mostafa Dehghani, Matthias Minderer, Georg Heigold, Sylvain Gelly, et al. An image is worth 16x16 words: Transformers for image recognition at scale. *arXiv preprint arXiv:2010.11929*, 2020. 1
- [7] Vincent Dumoulin, Jonathon Shlens, and Manjunath Kudlur. A learned representation for artistic style. In *International Conference on Learning Representations*, 2016. 2, 3, 4
- [8] Mohammad Fahes, Tuan-Hung Vu, Andrei Bursuc, Patrick Pérez, and Raoul de Charette. Poda: Prompt-driven zero-shot domain adaptation. In *Proceedings of the IEEE/CVF International Conference on Computer Vision*, pages 18623–18633, 2023. 3, 5
- [9] Rinon Gal, Or Patashnik, Haggai Maron, Amit H Bermano, Gal Chechik, and Daniel Cohen-Or. Stylegan-nada: Clip-guided domain adaptation of image generators. *ACM Transactions on Graphics (TOG)*, 41(4):1–13, 2022. 3, 5
- [10] Yaroslav Ganin and Victor Lempitsky. Unsupervised domain adaptation by backpropagation. In *International conference on machine learning*, pages 1180–1189. PMLR, 2015. 1
- [11] Leon A Gatys, Alexander S Ecker, and Matthias Bethge. Image style transfer using convolutional neural networks. In *Proceedings of the IEEE conference on computer vision and pattern recognition*, pages 2414–2423, 2016. 3, 4, 5
- [12] Leon A Gatys, Alexander S Ecker, Matthias Bethge, Aaron Hertzmann, and Eli Shechtman. Controlling perceptual factors in neural style transfer. In *Proceedings of the IEEE conference on computer vision and pattern recognition*, pages 3985–3993, 2017. 3
- [13] Taesik Gong, Jongheon Jeong, Taewon Kim, Yewon Kim, Jinwoo Shin, and Sung-Ju Lee. Note: Robust continual test-time adaptation against temporal correlation. *Advances in Neural Information Processing Systems*, 35:27253–27266, 2022. 2, 3
- [14] Kaiming He, Xiangyu Zhang, Shaoqing Ren, and Jian Sun. Deep residual learning for image recognition. In *Proceedings of the IEEE conference on computer vision and pattern recognition*, pages 770–778, 2016. 1
- [15] Dan Hendrycks and Thomas Dietterich. Benchmarking neural network robustness to common corruptions and perturbations. In *International Conference on Learning Representations*, 2018. 6, 8, 3
- [16] Xun Huang and Serge Belongie. Arbitrary style transfer in real-time with adaptive instance normalization. In *Proceedings of the IEEE/CVF International Conference on Computer Vision*, pages 1501–1510, 2017. 2, 3, 4, 5
- [17] Sergey Ioffe and Christian Szegedy. Batch normalization: Accelerating deep network training by reducing internal covariate shift. In *International conference on machine learning*, pages 448–456. pmlr, 2015. 3
- [18] Alex Krizhevsky. Learning multiple layers of features from tiny images. Master’s thesis, University of Toronto, 2009. 8, 3
- [19] Jungsoo Lee, Debasmit Das, Jaegul Choo, and Sungha Choi. Towards open-set test-time adaptation utilizing the wisdom of crowds in entropy minimization. In *Proceedings of the IEEE/CVF International Conference on Computer Vision*, pages 16380–16389, 2023. 2, 3
- [20] Yijun Li, Chen Fang, Jimei Yang, Zhaowen Wang, Xin Lu, and Ming-Hsuan Yang. Universal style transfer via feature transforms. *Advances in neural information processing systems*, 30, 2017. 3
- [21] Yanghao Li, Naiyan Wang, Jiaying Liu, and Xiaodi Hou. Demystifying neural style transfer. In *Proceedings of the 26th International Joint Conference on Artificial Intelligence*, pages 2230–2236, 2017. 3, 4, 5
- [22] Hyesu Lim, Byeongeun Kim, Jaegul Choo, and Sungha Choi. Ttn: A domain-shift aware batch normalization in test-time adaptation. In *The Eleventh International Conference on Learning Representations*, 2022. 2, 3
- [23] Yuejiang Liu, Parth Kothari, Bastien van Delft, Baptiste Bellot-Gurlet, Taylor Mordan, and Alexandre Alahi. Ttt++: When does self-supervised test-time training fail or thrive? In *Advances in Neural Information Processing Systems*, pages 21808–21820. Curran Associates, Inc., 2021. 1
- [24] Mingsheng Long, Yue Cao, Jianmin Wang, and Michael Jordan. Learning transferable features with deep adaptation networks. In *International conference on machine learning*, pages 97–105. PMLR, 2015. 1
- [25] Mingsheng Long, Han Zhu, Jianmin Wang, and Michael I Jordan. Unsupervised domain adaptation with residual transfer networks. *Advances in neural information processing systems*, 29, 2016. 1
- [26] Claudio Michaelis, Benjamin Mitzkus, Robert Geirhos, Evgenia Rusak, Oliver Bringmann, Alexander S Ecker, Matthias Bethge, and Wieland Brendel. Benchmarking ro-



- bustness in object detection: Autonomous driving when winter is coming. *arXiv preprint arXiv:1907.07484*, 2019. 6
- [27] Zachary Nado, Shreyas Padhy, D. Sculley, Alexander D’Amour, Balaji Lakshminarayanan, and Jasper Snoek. Evaluating prediction-time batch normalization for robustness under covariate shift, 2021. 2, 5, 6, 8
- [28] Shuaicheng Niu, Jiaxiang Wu, Yifan Zhang, Yaofu Chen, Shijian Zheng, Peilin Zhao, and Mingkui Tan. Efficient test-time model adaptation without forgetting. In *International conference on machine learning*, pages 16888–16905. PMLR, 2022. 1, 2, 3, 5, 6, 7
- [29] Shuaicheng Niu, Jiaxiang Wu, Yifan Zhang, Zhiquan Wen, Yaofu Chen, Peilin Zhao, and Mingkui Tan. Towards stable test-time adaptation in dynamic wild world. In *The Eleventh International Conference on Learning Representations*, 2023. 1, 2, 3
- [30] Sinno Jialin Pan, Ivor W Tsang, James T Kwok, and Qiang Yang. Domain adaptation via transfer component analysis. *IEEE transactions on neural networks*, 22(2):199–210, 2010. 1
- [31] Sunghyun Park, Seunghan Yang, Jaegul Choo, and Sungrack Yun. Label shift adapter for test-time adaptation under covariate and label shifts. In *Proceedings of the IEEE/CVF International Conference on Computer Vision*, pages 16421–16431, 2023. 2, 3
- [32] Or Patashnik, Zongze Wu, Eli Shechtman, Daniel Cohen-Or, and Dani Lischinski. Styleclip: Text-driven manipulation of stylegan imagery. In *Proceedings of the IEEE/CVF International Conference on Computer Vision*, pages 2085–2094, 2021. 5
- [33] Vishal M Patel, Raghuraman Gopalan, Ruonan Li, and Rama Chellappa. Visual domain adaptation: A survey of recent advances. *IEEE signal processing magazine*, 32(3):53–69, 2015. 1
- [34] Christos Sakaridis, Dengxin Dai, and Luc Van Gool. Acdc: The adverse conditions dataset with correspondences for semantic driving scene understanding. In *Proceedings of the IEEE/CVF International Conference on Computer Vision*, pages 10765–10775, 2021. 5
- [35] Steffen Schneider, Evgenia Rusak, Luisa Eck, Oliver Bringmann, Wieland Brendel, and Matthias Bethge. Improving robustness against common corruptions by covariate shift adaptation. *Advances in neural information processing systems*, 33:11539–11551, 2020. 2, 5, 3
- [36] Junha Song, Jungsoo Lee, In So Kweon, and Sungha Choi. Ecotta: Memory-efficient continual test-time adaptation via self-distilled regularization. In *Proceedings of the IEEE/CVF Conference on Computer Vision and Pattern Recognition (CVPR)*, pages 11920–11929, 2023. 1, 2, 3, 5, 6, 7
- [37] Yu Sun, Eric Tzeng, Trevor Darrell, and Alexei A Efros. Unsupervised domain adaptation through self-supervision. *arXiv preprint arXiv:1909.11825*, 2019. 1
- [38] Yu Sun, Xiaolong Wang, Zhuang Liu, John Miller, Alexei Efros, and Moritz Hardt. Test-time training with self-supervision for generalization under distribution shifts. In *International conference on machine learning*, pages 9229–9248. PMLR, 2020. 1
- [39] Yi-Hsuan Tsai, Wei-Chih Hung, Samuel Schuster, Kihyuk Sohn, Ming-Hsuan Yang, and Manmohan Chandraker. Learning to adapt structured output space for semantic segmentation. In *Proceedings of the IEEE conference on computer vision and pattern recognition*, pages 7472–7481, 2018. 1
- [40] Dmitry Ulyanov, Vadim Lebedev, Andrea Vedaldi, and Victor Lempitsky. Texture networks: Feed-forward synthesis of textures and stylized images. *arXiv preprint arXiv:1603.03417*, 2016. 3
- [41] Dequan Wang, Evan Shelhamer, Shaoteng Liu, Bruno Olshausen, and Trevor Darrell. Tent: Fully test-time adaptation by entropy minimization. In *International Conference on Learning Representations*, 2021. 1, 2, 3, 5, 6, 7, 8
- [42] Li Wang, Dong Li, Yousong Zhu, Lu Tian, and Yi Shan. Dual super-resolution learning for semantic segmentation. In *Proceedings of the IEEE/CVF Conference on Computer Vision and Pattern Recognition (CVPR)*, pages 3774–3783, 2020. 2
- [43] Qin Wang, Olga Fink, Luc Van Gool, and Dengxin Dai. Continual test-time domain adaptation. In *Proceedings of the IEEE/CVF Conference on Computer Vision and Pattern Recognition (CVPR)*, pages 7201–7211, 2022. 1, 2, 3, 5, 6, 8
- [44] Wei Wang, Zhun Zhong, Weijie Wang, Xi Chen, Charles Ling, Boyu Wang, and Nicu Sebe. Dynamically instance-guided adaptation: A backward-free approach for test-time domain adaptive semantic segmentation. In *Proceedings of the IEEE/CVF Conference on Computer Vision and Pattern Recognition*, pages 24090–24099, 2023. 2
- [45] Sergey Zagoruyko and Nikos Komodakis. Wide residual networks. In *Proceedings of the British Machine Vision Conference 2016*. British Machine Vision Association, 2016. 8, 3
- [46] Marvin Zhang, Sergey Levine, and Chelsea Finn. Memo: Test time robustness via adaptation and augmentation. *Advances in Neural Information Processing Systems*, 35: 38629–38642, 2022. 2
- [47] Yexun Zhang, Ya Zhang, and Wenbin Cai. Separating style and content for generalized style transfer. In *Proceedings of the IEEE conference on computer vision and pattern recognition*, pages 8447–8455, 2018. 3, 5
- [48] Hengshuang Zhao, Xiaojuan Qi, Xiaoyong Shen, Jianping Shi, and Jiaya Jia. Icnnet for real-time semantic segmentation on high-resolution images. In *Proceedings of the European conference on computer vision (ECCV)*, pages 405–420, 2018. 2



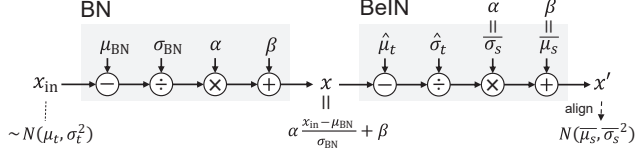


Figure B. BeIN overview, where BeIN is inserted after a BN layer.

$$\text{BeIN}(x) = \bar{\sigma}_s \cdot \frac{x - \hat{\mu}_t}{\hat{\sigma}_t} + \bar{\mu}_s \quad (\text{Ea})$$

$$\approx TTA(x) \sim N(\bar{\mu}_s, \bar{\sigma}_s^2) \quad (\text{Eb})$$

The objective of BeIN is to align the input distribution to the source distribution  $N(\bar{\mu}_s, \bar{\sigma}_s^2)$ , as shown in Eq. Eb. In our implementation, the objective statistics  $\bar{\sigma}_s = \alpha$  and  $\bar{\mu}_s = \beta$  since the BeIN layer is inserted after a BN layer as shown in Fig. B. Let  $x_{\text{in}} \in \mathbb{R}^{C \times HW}$  be the input before the BN layer that follows  $N(\mu_t, \sigma_t^2)$ . Then the input of the BeIN layer  $x = \text{BN}(x_{\text{in}}) = \alpha(x_{\text{in}} - \mu_{\text{BN}})/\sigma_{\text{BN}} + \beta$ , where  $(\mu_{\text{BN}}, \sigma_{\text{BN}})$  is the statistics of the source domain on which the BN layer is trained. The ideal BN aligned to the target domain is  $\text{BN}_{\text{ideal}}(x_{\text{in}}) = \alpha(x_{\text{in}} - \mu_t)/\sigma_t + \beta$ . Consequently, the objective of BeIN is formulated as follows:

$$\text{BeIN}(x) = \text{BeIN}(\text{BN}(x_{\text{in}})) = \text{BN}_{\text{ideal}}(x_{\text{in}}) \quad (\text{F})$$

A possible solution of Eq. F is as follows:

$$\hat{\sigma}_t = \frac{\sigma_t}{\sigma_{\text{BN}}} \alpha, \quad \hat{\mu}_t = \alpha \frac{\mu_t - \mu_{\text{BN}}}{\sigma_{\text{BN}}} + \beta \quad (\text{G})$$

Since the target statistics  $(\mu_t, \sigma_t)$  are unknown, we need to estimate the statistics based on other known statistics. To ensure stability, we estimate the statistics using the stable source statistics as an anchor point, instead of solely relying on the unstable sample statistics.

**Standard deviation** Let  $v = (x_{\text{in}} - \mu_t)/\sigma_t \sim N(0, 1)$  (i.e.,  $x_{\text{in}} = \mu_t + v\sigma_t$ .) Then the sample statistics are as follows:

$$\sigma_x = \alpha \sigma(v) \frac{\sigma_t}{\sigma_{\text{BN}}}, \quad \mu_x = \alpha \frac{\mu(v)\sigma_t + \mu_t - \mu_{\text{BN}}}{\sigma_{\text{BN}}} + \beta \quad (\text{H})$$

where  $\mu(v)$  and  $\sigma(v)$  are the mean and standard variation of  $v$ , respectively. By Eq. G and Eq. H, the optimal target statistics  $(\hat{\mu}_t, \hat{\sigma}_t)$  are as follows:

$$\hat{\sigma}_t = \frac{\sigma_x}{\sigma(v)}, \quad \hat{\mu}_t = \mu_x - \mu(v)\hat{\sigma}_t \quad (\text{I})$$

We approximate  $\sigma(v) = \sigma_x/\hat{\sigma}_t$  by the weighted sum of the ideal case ( $\sigma(v) = 1$ ) and the source-sample deviation difference  $\sigma_x/\bar{\sigma}_s$  with a learnable parameter  $\gamma'_\sigma$ :

$$\sigma(v) \simeq \rho + (1 - \rho) \frac{\sigma_x}{\bar{\sigma}_s} + \gamma'_\sigma \quad (\text{J})$$

Method	Batch size		
	1	2	4
Source	41.8	41.8	41.8
TENT-continual [41]	37.3	40.1	41.3
EATA [28]	37.4	39.2	39.6
CoTTA [43]	42.6	42.8	42.9
EcoTTA [36]	37.4	38.0	38.4
PETAL [1]	41.8	42.0	42.0
<b>BESTTA (Ours)</b>	<b>44.2</b>	<b>44.2</b>	<b>44.1</b>

Table A. Ablation study on batch sizes. Performances (mIoU in %) are evaluated on Cityscapes-to-ACDC continual test-time adaptation task, using DeepLabV3Plus-ResNet50 [3]. Input images are resized to  $960 \times 540$ . Our proposed method consistently achieves the highest performance regardless of batch sizes.

Therefore, by Eq. I and Eq. J,

$$\frac{1}{\hat{\sigma}_t} = \frac{\rho}{\sigma_x} + \frac{1 - \rho}{\bar{\sigma}_s} + \frac{\gamma'_\sigma}{\sigma_x} \quad (\text{Ka})$$

$$\iff \hat{\sigma}_t = \frac{\bar{\sigma}_s \cdot \sigma_x}{\rho \bar{\sigma}_s + (1 - \rho)\sigma_x + \gamma_\sigma} \quad (\text{Kb})$$

Eq. Kb is equivalent to Eq. 7, where  $\gamma_\sigma = \bar{\sigma}_s \gamma'_\sigma$  for simplicity.

**Mean** Similar to  $\sigma(v)$ , we approximate  $\mu(v) = (\mu_x - \hat{\mu}_t)/\hat{\sigma}_t$  by the weighted sum of the ideal case ( $\mu(v) = 0$ ) and the source-sample mean difference  $(\mu_x - \bar{\mu}_s)/\bar{\mu}_s$  with a learnable parameter  $\gamma'_\mu$ .

$$\mu(v) \simeq (1 - \rho) \frac{\mu_x - \bar{\mu}_s}{\bar{\mu}_s} + \gamma'_\mu \quad (\text{L})$$

Therefore, by Eq. J and Eq. L,

$$\hat{\mu}_t = \mu_x - \mu(v)\hat{\sigma}_t \quad (\text{Ma})$$

$$= \hat{\sigma}_t \left( \frac{\mu_x}{\sigma_x} \sigma(v) - \mu(v) \right) \quad (\text{Mb})$$

$$\simeq \hat{\sigma}_t \left( \rho \frac{\mu_x}{\sigma_x} + (1 - \rho) \frac{\bar{\mu}_s}{\bar{\sigma}_s} + \frac{\mu_x}{\sigma_x} \gamma'_\sigma - \gamma'_\mu \right) \quad (\text{Mc})$$

$$= \rho \frac{\hat{\sigma}_t}{\sigma_x} \cdot \mu_x + (1 - \rho) \frac{\hat{\sigma}_t}{\bar{\sigma}_s} \cdot \bar{\mu}_s + \gamma_\mu \quad (\text{Md})$$

Eq. Md is equivalent to Eq. 8, where  $\gamma_\mu = \frac{\mu_x}{\sigma_x} \gamma'_\sigma - \gamma'_\mu$  for simplicity.

## B. Additional ablation studies

We provide additional ablation studies and the complete results of the ablations studies in Sec. 4.1.

**Effectiveness of batch sizes.** We evaluate our method and the baselines on batch sizes of 1, 2, and 4. Table A shows that our method consistently performs better than the

baselines, demonstrating its robustness to batch sizes. The BN-based methods (TENT-continual [41], EATA [28], and EcoTTA [36]) improve with larger batch sizes due to reduced instability, whereas CoTTA [43] and PETAL [1] do not exhibit significant improvement. Despite their improved performance, our method consistently surpasses the baselines regardless of the batch sizes.

**Effectiveness of losses.** Table B displays the complete results of the ablation study on losses in Table 4. The results indicate that the proposed losses presented in Sec. 3.3 effectively enables the single-image continual test-time adaptation as follows. Firstly, the style loss outperforms the entropy loss, confirming its effectiveness. Secondly, using both the style loss and the entropy enhances the performance, indicating the stability of the style loss. Thirdly, the use of content loss consistently improves the performance, indicating the effectiveness of the content loss. Lastly, the L2 regularization loss helps performance by preventing the catastrophic forgetting, which is especially effective when used with the style loss and the content loss.

**Layer selection to insert BeIN Layer.** Table C provides the complete results of the ablation study on the layer selection to insert the proposed BeIN layer in Table 5. The results indicate that inserting the BeIN layer after *Layer3* consistently performs better than other cases in terms of mIoU in each round, regardless of the number of BeIN layers used. Additionally, inserting a BeIN layer after *Layer1* achieves better adaptation performance in fog and snow condition, as presented in (e), (f), and (m). This result indicates that selecting a layer in the lower level is advantageous in the presence of prevalent adverse weather effects, as the low-level features capture the prevalent patterns [8]. The results suggest that inserting a BeIN layer following a higher-level layer, excluding the last layer, is more effective. This is due to the ability of the higher-level layers to capture the global adverse weather effects such as rain accumulation.

Notably, using a single BeIN layer after *Layer3* achieves the highest performance, as demonstrated in (c). This implies that *Layer3* captures both low- and high-level features, enabling effective style transfer guided adaptation. However, using more BeIN layers does not improve performance, as shown in (e-o). We speculate that the normalization process becomes unstable when transferring the style more than once.

## C. Complete implementation details

We provide further implementation details for our experiments in Sec. 4.

**Details for the correlations** To examine the correlations between adaptation performance and style transfer related metrics in Fig. 3 and Fig. C, we measure direction similarity, target similarity, entropy, and source similarity, which

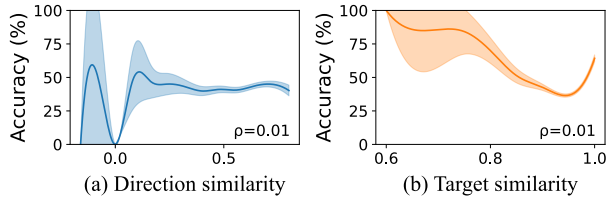


Figure C. Correlations between performance and style transfer related metrics in image classification. In contrast to semantic segmentation, we discover that direction and target similarities are uncorrelated ( $\rho < 0.05$ ). Target similarity appears to be related in (b), however, the majority of data (93.7%) have target similarity above 0.9, making the results unreliable. All results are evaluated on CIFAR-10-C [15] using WideResNet-28 [45] pretrained on CIFAR-10 [18].

are described in Sec. 3.3. We measure the similarities between adapted and unadapted embeddings, using the method suggested by Schneider *et al.* [35], a simple unsupervised adaptation method that employs the weighted mean of batch statistics derived from both the source and target data. We set the hyperparameter  $N$  to 8, as suggested by the authors, where  $N$  determines the weights for the source and target statistics. The colored regions in Fig. 3 and Fig. C indicate the 95% confidence interval.

**Details for image classification** In the image classification experiments in Sec. 4.2, we set the learning rate to 0.1,  $\rho$  to 0.9 and  $\lambda_1, \lambda_2, \lambda_3,$  and  $\lambda_4$  to 1, 0, 1, and 0, respectively. Based on our empirical observations depicted in Fig. C, the content loss is not effective in image classification, thus, we do not utilize it in image classification. This is because the image classification data are synthetic, the content of the data remains unchanged in the presence of image corruption. We replace the style loss with the cosine distance between  $\mathcal{E}(x_{src})$  and  $\mathcal{E}'(x)$ , i.e.  $\mathcal{L}_{style} = 1 - \cos(\mathcal{E}(x_{src}), \mathcal{E}'(x))$ . We find that employing this straightforward form of style loss is more effective in guiding the BeIN layer to successfully transfer the style of the input image in image classification.

**Other details** In Sec. 4.1, we set  $\rho$  to 0.7 and set the momentum value of the optimizer to 0.9. For baselines, we use the optimal configurations provided in their respective papers. We measure the peak GPU memory consumption using `torch.cuda.max_memory_allocated()` method. We measure the average processing time per image by averaging the wall time elapsed for processing 1,000 images. The average processing time includes both the forward and backward operations.

## D. Further experimental results

We present the further experimental results including the complete results of the experiments in Sec. 4.

	$\mathcal{L}_{entropy}$	$\mathcal{L}_{style}$	$\mathcal{L}_{content}$	$\mathcal{L}_{L2}$	Round 1	Round 4	Round 7	Round 10	Mean
(a)	✓	✗	✗	✗	21.2	5.3	4.5	4.2	6.7
(b)	✗	✓	✗	✗	31.0	25.4	24.4	24.0	25.6
(c)	✓	✓	✗	✗	37.1	32.3	30.2	28.9	31.8
(d)	✓	✗	✓	✗	21.8	14.0	13.6	13.4	14.7
(e)	✓	✗	✗	✓	13.8	5.0	5.0	5.0	5.9
(f)	✗	✓	✓	✗	39.0	37.3	37.1	36.9	37.4
(g)	✗	✓	✗	✓	38.3	38.6	38.5	38.6	38.5
(h)	✓	✓	✓	✗	40.1	39.2	37.9	37.3	38.6
(i)	✓	✓	✗	✓	28.8	26.9	26.9	26.9	27.1
(j)	✓	✗	✓	✓	37.2	41.1	41.1	41.1	40.7
(k)	✗	✓	✓	✓	40.4	40.7	40.7	40.8	40.7
(l)	✓	✓	✓	✓	<b>40.8</b>	<b>43.5</b>	<b>43.6</b>	<b>43.6</b>	<b>43.2</b>

Table B. Ablation study on our losses. Performances (mIoU in %) are evaluated on Cityscapes-to-ACDC single image continual test-time adaptation task for each different combination of losses, using DeepLabV3Plus-ResNet50 [3]. The results are separated by the number of losses used. Using all of our proposed losses considerably improves the performance. Because the content loss and the L2 regularization are only meaningful with other losses, their individual results are excluded.

	Layer1	Layer2	Layer3	Layer4	Fog	Night	Rain	Snow	Round 1	Round 4	Round 7	Round 10	Mean
(a)	✓	✗	✗	✗	53.6	22.2	46.5	44.4	40.2	42.0	41.9	41.9	41.7
(b)	✗	✓	✗	✗	52.6	21.8	45.9	43.4	39.3	41.1	41.1	41.1	40.9
(c)	✗	✗	✓	✗	<u>53.7</u>	<u>26.0</u>	<b>48.3</b>	45.0	<b>40.8</b>	<b>43.5</b>	<b>43.6</b>	<b>43.6</b>	<b>43.2</b>
(d)	✗	✗	✗	✓	42.1	23.5	40.2	38.1	36.0	36.0	36.0	36.0	36.0
(e)	✓	✓	✗	✗	54.2	17.8	47.5	44.9	39.7	41.2	41.2	41.2	41.1
(f)	✓	✗	✓	✗	<b>54.3</b>	23.3	48.2	<u>46.2</u>	38.7	<b>43.5</b>	<u>43.5</u>	<u>43.5</u>	<u>43.0</u>
(g)	✓	✗	✗	✓	47.7	<b>26.1</b>	45.2	42.6	40.1	40.4	40.4	40.4	40.4
(h)	✗	✓	✓	✗	52.5	23.2	46.5	44.7	39.6	42.0	41.9	41.9	41.7
(i)	✗	✓	✗	✓	49.6	25.3	44.3	41.9	39.1	40.4	40.4	40.4	40.3
(j)	✗	✗	✓	✓	51.9	25.0	45.8	42.8	39.0	41.6	41.6	41.6	41.4
(k)	✓	✓	✓	✗	53.0	23.0	47.0	45.4	38.4	42.5	42.5	42.5	42.1
(l)	✓	✓	✗	✓	51.2	21.0	45.4	43.7	39.2	40.5	40.4	40.4	40.3
(m)	✓	✗	✓	✓	53.2	25.3	<u>47.3</u>	<b>46.3</b>	40.0	<u>43.4</u>	43.3	43.4	<u>43.0</u>
(n)	✗	✓	✓	✓	51.3	23.5	45.5	43.9	38.1	41.4	41.4	41.4	41.0
(o)	✓	✓	✓	✓	52.0	23.6	46.5	45.2	38.5	42.2	42.1	42.2	41.8

Table C. Ablation study on the position of BeIN. Performances (mIoU in %) are evaluated on Cityscapes-to-ACDC single image continual test-time adaptation task, using DeepLabV3Plus-ResNet50 [3]. The results are separated by the number of layers where BeIN is inserted.

**Complete results** Table D presents the complete results of Table 2. Our method consistently outperforms the baselines in all rounds regardless of the weather conditions on the Cityscapes-to-ACDC single image continual test-time adaptation task. Our method consumes the lowest GPU memory and the second lowest processing time among the backward-based baseline test-time adaptation methods. Table E shows the complete results of Table 3. Our method achieves the highest mean mIoU regardless of the type of corruptions on the Cityscapes-to-Cityscapes-C single image gradual test-time adaptation task.

**Further qualitative results** Fig. D illustrates the distributions of adapted embeddings of our method and the baselines in each channel. Our method effectively aligns the embedding distribution with the source distribution, irrespective of the weather conditions, demonstrating the effectiveness and stability of our method. On the contrary, the BN-based methods exhibit instability as their embedding distributions collapse to a single point. Fig. E presents further predictions of our method and the baselines. Our method consistently outperforms the baselines across the weather conditions, with higher accuracy and lower noise.



Time	$t \longrightarrow$																			
Method	Round 1					Round 2					Round 3					Round 4				
	Fog	Night	Rain	Snow	Mean	Fog	Night	Rain	Snow	Mean	Fog	Night	Rain	Snow	Mean	Fog	Night	Rain	Snow	Mean
Source	44.3	22.0	41.5	38.9	36.6	44.3	22.0	41.5	38.9	36.6	44.3	22.0	41.5	38.9	36.6	44.3	22.0	41.5	38.9	36.6
BN Stats Adapt [27]	36.8	23.5	38.2	36.3	33.7	36.8	<u>23.5</u>	38.2	36.3	33.7	36.8	<u>23.5</u>	38.2	36.3	33.7	36.8	23.5	38.2	36.3	33.7
TENT* [41]	38.2	22.9	41.1	37.8	35.0	38.2	22.9	41.1	37.8	35.0	38.2	22.9	41.1	37.8	35.0	38.2	22.9	41.1	37.8	35.0
TENT-continual [41]	37.7	<u>23.5</u>	39.9	37.5	34.6	39.0	22.1	37.6	34.0	33.2	35.5	19.9	34.3	30.3	30.0	31.4	17.3	30.7	26.8	26.6
EATA [28]	36.8	23.4	38.3	36.5	33.7	37.1	23.4	38.5	36.7	33.9	37.3	23.5	38.8	36.9	34.1	37.6	<u>23.5</u>	39.0	37.1	34.3
CoTTA [43]	<u>46.3</u>	22.0	<u>44.2</u>	<u>40.4</u>	<u>38.2</u>	<u>47.3</u>	21.7	<u>45.0</u>	40.4	<u>38.6</u>	<u>47.8</u>	21.4	<u>45.3</u>	40.3	<u>38.7</u>	<u>48.1</u>	21.0	<u>45.3</u>	40.2	38.6
EcoTTA [36]	33.4	20.8	35.6	32.9	30.7	33.7	21.0	35.8	33.0	30.9	34.0	21.1	35.9	33.1	31.0	34.2	21.2	36.1	33.2	31.1
PETAL [1]	44.7	22.1	42.9	40.1	37.5	46.6	22.4	43.8	<u>40.6</u>	38.4	47.2	22.4	44.2	<u>40.7</u>	38.6	47.3	22.4	44.4	<u>40.8</u>	<u>38.7</u>
BESTTA (Ours)	<b>47.8</b>	<b>24.3</b>	<b>47.2</b>	<b>43.8</b>	<b>40.8</b>	<b>53.4</b>	<b>26.3</b>	<b>48.3</b>	<b>44.8</b>	<b>43.2</b>	<b>54.3</b>	<b>26.2</b>	<b>48.4</b>	<b>45.1</b>	<b>43.5</b>	<b>54.5</b>	<b>26.1</b>	<b>48.4</b>	<b>45.2</b>	<b>43.5</b>

(a) Round 1–4

Time	$t \longrightarrow$																			
Method	Round 5					Round 6					Round 7					Round 8				
	Fog	Night	Rain	Snow	Mean	Fog	Night	Rain	Snow	Mean	Fog	Night	Rain	Snow	Mean	Fog	Night	Rain	Snow	Mean
Source	44.3	22.0	41.5	38.9	36.6	44.3	22.0	41.5	38.9	36.6	44.3	22.0	41.5	38.9	36.6	44.3	22.0	41.5	38.9	36.6
BN Stats Adapt [27]	36.8	23.5	38.2	36.3	33.7	36.8	23.5	38.2	36.3	33.7	36.8	23.5	38.2	36.3	33.7	36.8	23.5	38.2	36.3	33.7
TENT* [41]	38.2	22.9	41.1	37.8	35.0	38.2	22.9	41.1	37.8	35.0	38.2	22.9	41.1	37.8	35.0	38.2	22.9	41.1	37.8	35.0
TENT-continual [41]	27.2	14.7	26.6	23.4	23.0	23.1	12.7	22.6	20.2	19.7	19.8	11.2	18.8	17.3	16.8	17.2	10.1	15.9	15.0	14.5
EATA [28]	37.7	<u>23.5</u>	39.2	37.3	34.4	37.9	<u>23.5</u>	39.4	37.5	34.6	38.1	<u>23.6</u>	39.5	37.6	34.7	38.2	<u>23.6</u>	39.7	37.8	34.8
CoTTA [43]	<u>48.1</u>	20.8	<u>45.4</u>	40.0	38.6	<u>48.1</u>	20.5	<u>45.3</u>	39.9	38.5	<u>48.1</u>	20.4	<u>45.3</u>	39.7	38.4	<u>48.1</u>	20.2	<u>45.2</u>	39.6	38.3
EcoTTA [36]	34.4	21.2	36.2	33.2	31.3	34.5	21.3	36.3	33.2	31.3	34.7	21.3	36.3	33.2	31.4	34.8	21.4	36.4	33.2	31.4
PETAL [1]	47.3	22.3	44.5	<u>40.7</u>	<u>38.7</u>	47.3	22.2	44.6	<u>40.6</u>	<u>38.7</u>	47.1	22.1	44.7	<u>40.6</u>	<u>38.6</u>	47.1	22.0	44.6	<u>40.6</u>	<u>38.6</u>
BESTTA (Ours)	<b>54.5</b>	<b>26.1</b>	<b>48.4</b>	<b>45.2</b>	<b>43.6</b>	<b>54.5</b>	<b>26.1</b>	<b>48.4</b>	<b>45.3</b>	<b>43.6</b>	<b>54.5</b>	<b>26.1</b>	<b>48.4</b>	<b>45.3</b>	<b>43.6</b>	<b>54.5</b>	<b>26.1</b>	<b>48.4</b>	<b>45.3</b>	<b>43.6</b>

(b) Round 5–8

Time	$t \longrightarrow$										Mean $\uparrow$ (%)	Time $\downarrow$ (ms)	Memory $\downarrow$ (GB)
Method	Round 9					Round 10							
	Fog	Night	Rain	Snow	Mean	Fog	Night	Rain	Snow	Mean			
Source	44.3	22.0	41.5	38.9	36.6	44.3	22.0	41.5	38.9	36.6	36.6	135.9	1.76
BN Stats Adapt [27]	36.8	23.5	38.2	36.3	33.7	36.8	23.5	38.2	36.3	33.7	33.7	192.7	2.01
TENT* [41]	38.2	22.9	41.1	37.8	35.0	38.2	22.9	41.1	37.8	35.0	35.0	343.8	<u>9.58</u>
TENT-continual [41]	15.1	9.3	13.9	13.2	12.9	13.4	8.7	12.4	11.8	11.6	22.3	343.8	<u>9.58</u>
EATA [28]	38.3	<u>23.6</u>	39.8	37.9	34.9	38.5	<u>23.6</u>	39.9	38.0	35.0	34.4	<b>190.6</b>	9.90
CoTTA [43]	<u>48.0</u>	20.1	<u>45.2</u>	39.6	38.2	<u>48.0</u>	20.0	<u>45.1</u>	39.5	38.1	38.4	4337	18.20
EcoTTA [36]	34.9	21.4	36.4	33.2	31.5	34.9	21.4	36.5	33.2	31.5	31.2	759.3	10.90
PETAL [1]	47.0	21.9	44.6	<u>40.5</u>	<u>38.5</u>	46.9	22.0	44.6	<u>40.5</u>	<u>38.5</u>	<u>38.5</u>	5120	18.51
BESTTA (Ours)	<b>54.5</b>	<b>26.1</b>	<b>48.4</b>	<b>45.3</b>	<b>43.6</b>	<b>54.5</b>	<b>26.1</b>	<b>48.4</b>	<b>45.3</b>	<b>43.6</b>	<b>43.2</b>	<u>291.8</u>	<b>8.77</b>

(c) Round 9–10

Table D. Semantic segmentation results (mIoU in %) on Cityscapes-to-ACDC single image continual test-time adaptation task. We compare ours with other state-of-the-art TTA methods in terms of peak GPU memory usage (GB) and time consumption (ms) for each iteration, and mean intersection over union (mIoU). All results are evaluated using the DeepLabV3Plus-ResNet50 [3]. \* denotes the requirement about when the domain shift occurs. The **best** and second best results among the backward-based methods are highlighted.

Time	$t \longrightarrow$									Mean
Severity	1	2	3	4	5	4	3	2	1	
Source	<b>73.2</b>	<b>71.1</b>	<u>67.7</u>	<u>63.1</u>	57.2	<u>63.1</u>	<u>67.7</u>	<b>71.1</b>	<b>73.2</b>	<u>67.5</u>
TENT-continual [41]	70.0	67.4	64.9	62.1	<u>58.8</u>	59.1	58.8	58.2	57.5	61.9
PETAL [1]	<u>73.1</u>	<u>70.8</u>	67.0	61.6	54.2	59.1	63.0	65.9	68.2	64.7
BESTTA (Ours)	72.9	70.7	<b>68.3</b>	<b>65.3</b>	<b>61.4</b>	<b>65.0</b>	<b>67.8</b>	<u>70.1</u>	<u>71.9</u>	<b>68.2</b>

(a) Brightness

Time	$t \longrightarrow$									Mean
Severity	1	2	3	4	5	4	3	2	1	
Source	<b>67.1</b>	<u>63.5</u>	<u>58.0</u>	<u>55.7</u>	<u>44.8</u>	<u>55.7</u>	<u>58.0</u>	<u>63.5</u>	<b>67.1</b>	<u>59.3</u>
TENT-continual [41]	53.5	50.9	48.2	45.3	40.7	42.0	42.2	42.1	42.0	45.2
PETAL [1]	58.0	50.7	41.3	32.5	17.8	25.6	28.7	31.9	36.2	35.8
BESTTA (Ours)	<u>66.5</u>	<b>64.0</b>	<b>59.6</b>	<b>57.6</b>	<b>50.4</b>	<b>57.2</b>	<b>59.3</b>	<b>63.6</b>	<u>66.1</u>	<b>60.5</b>

(b) Fog

Time	$t \longrightarrow$									Mean
Severity	1	2	3	4	5	4	3	2	1	
Source	<u>44.9</u>	25.6	18.0	16.3	13.5	16.3	18.0	<u>25.6</u>	<u>44.9</u>	<u>24.8</u>
TENT-continual [41]	33.8	<u>27.7</u>	<u>23.5</u>	<u>21.6</u>	<b>19.6</b>	<u>19.5</u>	<u>19.3</u>	20.1	21.6	23.0
PETAL [1]	17.7	6.6	4.5	3.6	3.1	3.0	3.2	3.3	6.0	5.7
BESTTA (Ours)	<b>53.8</b>	<b>38.4</b>	<b>28.1</b>	<b>24.1</b>	<u>17.9</u>	<b>20.5</b>	<b>21.9</b>	<b>30.1</b>	<b>49.6</b>	<b>31.6</b>

(c) Frost

Time	$t \longrightarrow$									Mean
Severity	1	2	3	4	5	4	3	2	1	
Source	<u>25.3</u>	11.8	11.5	9.1	9.5	9.1	11.5	11.8	<u>25.3</u>	13.9
TENT-continual [41]	19.3	<u>16.8</u>	<u>16.7</u>	<b>15.1</b>	<b>14.2</b>	<b>13.9</b>	<u>14.0</u>	<u>13.2</u>	14.2	<u>15.3</u>
PETAL [1]	0.7	0.5	0.3	0.3	0.5	0.3	0.3	0.3	0.4	0.4
BESTTA (Ours)	<b>39.5</b>	<b>20.4</b>	<b>18.6</b>	<u>12.8</u>	<u>12.5</u>	<u>12.2</u>	<b>16.0</b>	<b>16.9</b>	<b>30.7</b>	<b>20.0</b>

(d) Snow

Method	Source	TENT-continual [41]	PETAL [1]	BESTTA (Ours)
Mean mIoU (%)	<u>41.4</u>	36.3	26.7	<b>45.0</b>

(e) Mean

Table E. Semantic segmentation results (mIoU in %) on the Cityscapes-to-Cityscapes-C gradual test-time adaptation task. All experiments are evaluated using DeepLabV3Plus-ResNet50 [3]. The **best** and second best results are highlighted.

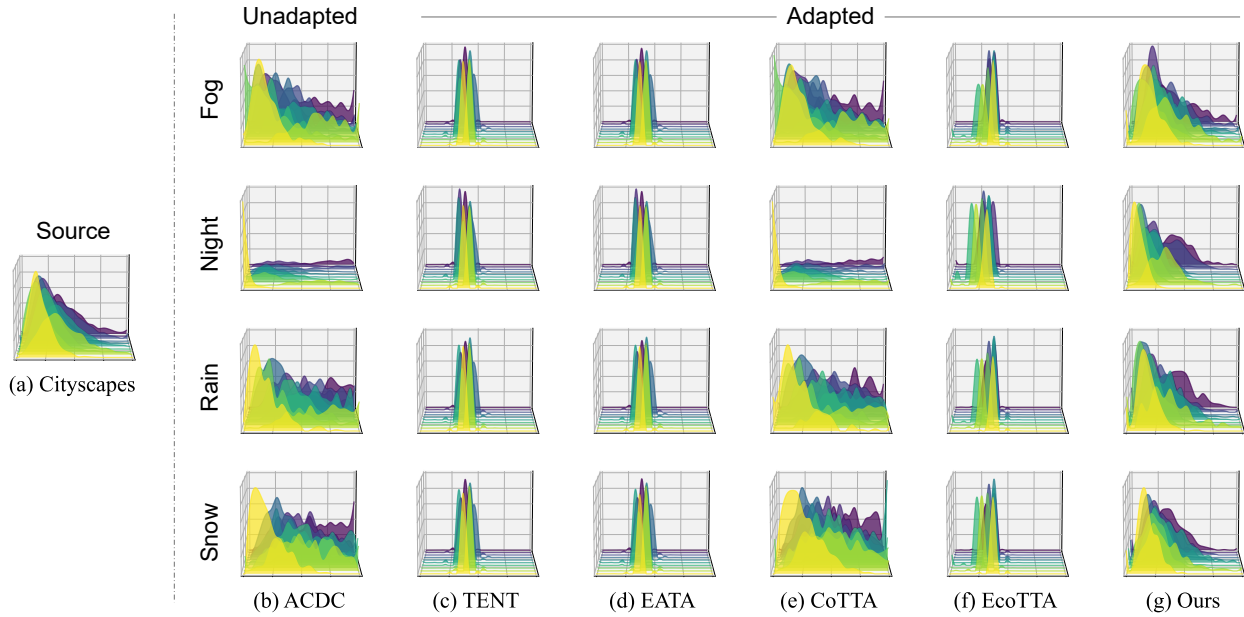


Figure D. Embedding feature distributions of adapted embeddings in our method and the baselines. Our method successfully aligns the target distribution (ACDC) to the source distribution (Cityscapes). Our method successfully aligns the embedding distribution with the source distribution, whereas the BN-based methods (TENT [41], EATA [28], EcoTTA [36]) exhibit instability as their embedding distributions collapse. We use DeepLabV3Plus-ResNet50 [3] pretrained on Cityscapes [5] in this experiment.

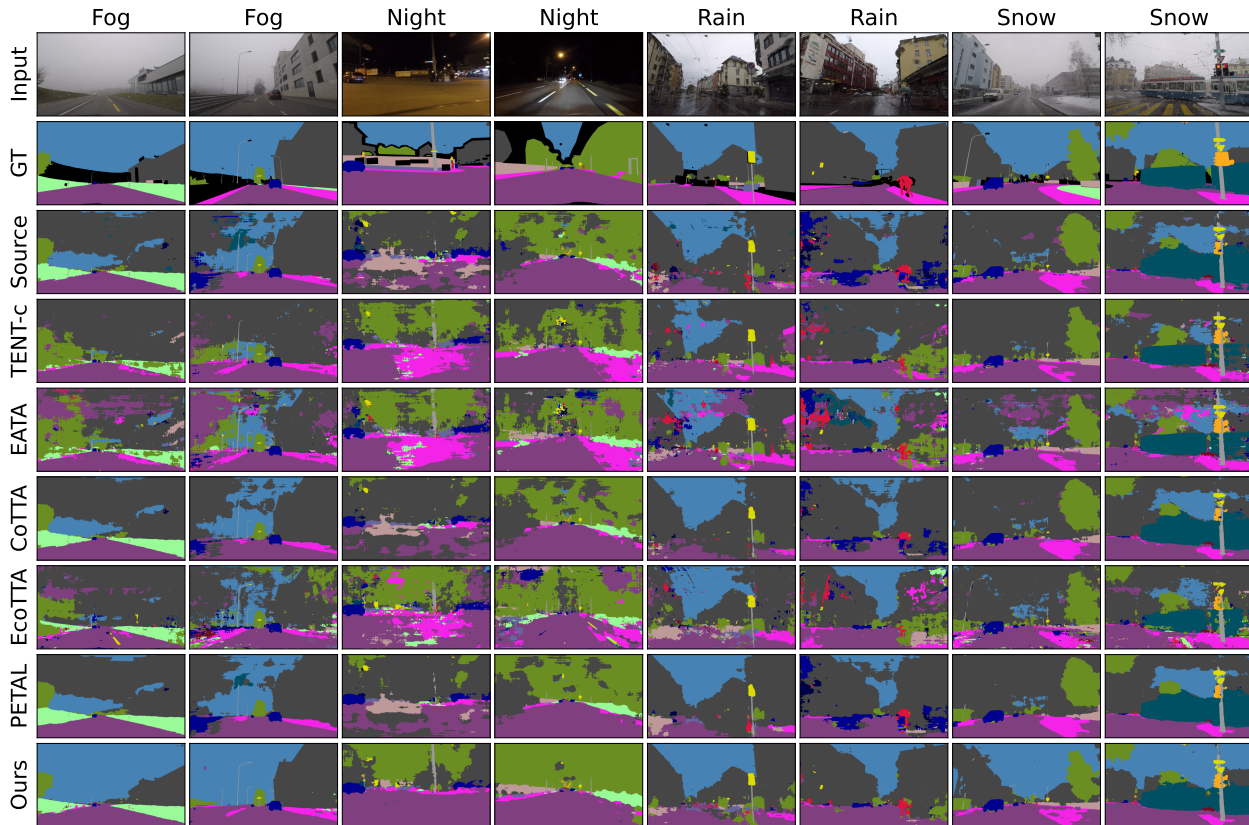


Figure E. Further qualitative comparison of semantic segmentation on Cityscapes-to-ACDC single image continual test-time adaptation task. All experiments are evaluated using DeepLabV3Plus-ResNet50 [3]. TENT-c denotes the TENT-continual [41] method.